

Disorder-induced symmetry lowering in the CsInMgF₆ pyrochlore crystal

A. P. Ayala, C. W. A. Paschoal, I. Guedes, W. Paraguassu, P. T. C. Freire, and J. Mendes Filho
Departamento de Física, Universidade Federal do Ceará, Caixa Postal 6030, 60451-970, Fortaleza, Ceará, Brazil

R. L. Moreira
Departamento de Física, ICEX, Universidade Federal de Minas Gerais, Caixa Postal 702, 30123-970, Belo Horizonte, Minas Gerais, Brazil

J.-Y. Gesland
Université du Maine-Cristallogène, URA 807, 72017-Le Mans Cedex, France
 (Received 11 April 2002; published 17 December 2002)

Polarized Raman scattering and infrared reflectivity of the modified pyrochlore single crystal CsInMgF₆ have been carried out at room temperature. The spectra showed the appearance of additional Raman and infrared bands, which are not predicted from group theory for the pyrochlore cubic structure. A deeper analysis, by taking into account the occupational disorder of Mg²⁺ and In³⁺ in octahedral sites, indicates that the overall features can be explained by a lowering of the crystal symmetry from $F\bar{3}m (O_h^7)$ to $R\bar{3}m (D_{3d}^5)$. This result should have important consequences on the understanding of the unusual magnetic behavior of this system.

DOI: 10.1103/PhysRevB.66.214105

PACS number(s): 78.30.Ly, 63.20.Dj, 63.50.+x

I. INTRODUCTION

In recent years, compounds that present a pyrochlore lattice have been object of several studies, due to their high probability of showing geometrical frustration. The origin of this effect can be understood by considering the possible vector spin configurations on the single trigonal and tetragonal units, for which no configuration can be simultaneously minimized for all bond energies. This kind of frustration is responsible by complex phenomena, such as spin-glass transitions, noncolinear and incommensurate ordering patterns, and unusual critical properties.¹⁻⁴

The pyrochlore structure has the form $A_2M_2X_6X'$ (where X and $X' = O, F, S, OH$) and can be viewed as an interpenetrated network of $octahedra and anticristobalite type A_2X' . This structure crystallizes in a face centered cubic lattice belonging to the $Fd\bar{3}m$ space group with eight formulas per unit cell. When the A_2X' sublattice is replaced by larger monovalent cations, such as Cs⁺ and Rb⁺, this structure is commonly designated as modified pyrochlore structure. Two great families of compounds are known to crystallize in these structures: oxides, with the formula $A_2^{3+}B_2^{4+}O_7$ (where A/B can be magnetic and A^{3+} is often a rare-earth ion) and fluorides, with the formula $AM^{2+}M'^{3+}F_6$ (where A is often an alkali-metal ion, and M^{2+} and M'^{3+} are usually transition-metal ions).$

From the structural point of view, the oxide family is well ordered, while in the majority of the compounds of the fluoride family, the M^{2+} and M'^{3+} ions are randomly distributed in the octahedral sites. As an exception to this rule, some compounds, such as $LiFe^{2+}Fe^{3+}F_6$,⁵ $NH_4Fe^{2+}Fe^{3+}F_6$,^{6,7} and NH_4CoAlF_6 (Ref. 8), are ordered but the symmetry is reduced to the space group $P4_2/mnm (D_{4h}^{14})$. Evidently, the magnetic properties of these compounds depend strongly of the distribution of the M^{2+} and M'^{3+} ions in the octahedral sites. In the disordered case,

such as CsMnFeF₆ (Ref. 9) and CsNiCrF₆,^{10,11} a spin glass behavior is observed, contradicting the antiferromagnetic ordering expected for the ordered structure.⁷

Although several studies of the magnetic properties of those materials have been accomplished, their vibrational properties have not been studied so far. In this work, we report on the vibrational spectra of modified pyrochlore CsInMgF₆ single-crystal at room temperature, using polarized Raman scattering and infrared reflectivity measurements. The main point of this work is to present a detailed analysis of the anomalous vibrational spectra based on the symmetry lowering due to the disorder of the M^{2+} and M'^{3+} ions. Our calculations allow us to predict not only the number and polarization dependence of the Raman and infrared active phonons but also the relative intensities of the Raman bands. The influence of the symmetry lowering on the magnetic properties of this material is briefly discussed at the end of Sec. V.

II. EXPERIMENTAL PROCEDURES

Single crystals of CsInMgF₆ were grown by Czochralski technique. The sample used in the Raman measurement, with dimensions of 3.0×3.0×3.0 mm³ was cut with faces perpendicular to the [110], $[1\bar{1}0]$, and [001] directions and was carefully polished with diamond paste. Raman spectra were recorded by using a Jobin-Yvon Triplemate Spectrometer (model T64000) equipped with a LN₂-cooled CCD detector. The spectra were taken in the backscattering configuration, using 50 mW of the 514.5 nm line of a Spectra Physics 170 Argon ion laser as exciting source. Scattering geometries for the spectra listed in the text and figures follow the usual Porto's notation $A(BC)D$.¹² Reflection infrared spectra were recorded with a BOMEM DA8 Fourier Transformer spectrometer, in the range 30 to 4000 cm⁻¹. The spectral resolution was typically 4 cm⁻¹. For the mid infrared region

TABLE I. Factor group analysis of the CsInMgF₆ crystal structure.

Ion	Wyckoff site	Symmetry	Irreducible representations
Cs ⁺	8b	T_d	$F_{1u} \oplus F_{2g}$
Mg ²⁺ /In ³⁺	16c	D_{3d}	$A_{2u} \oplus E_u \oplus 2F_{1u} \oplus F_{2u}$
F ⁻	48f	C_{2v}	$A_{1g} \oplus A_{2u} \oplus E_g \oplus E_u \oplus 2F_{1g} \oplus 3F_{1u} \oplus 3F_{2g} \oplus 2F_{2u}$
	Total		$\Gamma = A_{1g} \oplus 2A_{2u} \oplus 2E_u \oplus E_g \oplus 6F_{1u} \oplus 2F_{1g} \oplus 3F_{2u} \oplus 4F_{2g}$
	Acoustic		$\Gamma_{ac} = F_{1u}$
	Raman		$\Gamma_R = A_{1g} \oplus E_g \oplus 4F_{2g}$
	Infrared		$\Gamma_{IR} = 5F_{1u}$

(above 400 cm⁻¹), the best choice of accessories was: Globar source, coated KBr beamsplitter and LN₂-cooled HgCdTe detector. The far infrared region was measured using Globar or Mercurium arc lamp (below 200 cm⁻¹), 6 μm coated-mylar Hypersplitter™ and LHe-cooled Si bolometer.

III. CRYSTALLINE STRUCTURE AND FACTOR GROUP ANALYSIS

The modified pyrochlore $AM^{2+}M'^{3+}F_6$ has a face centered cubic structure belonging to $Fd\bar{3}m$ space group with eight molecules per unit cell (two molecules in the primitive cell). According to Hoopé,¹⁶ the A ions occupy special $8b$ Wyckoff sites, F ions the $48f$ sites, and M^{2+} and M'^{3+} ions occupy well defined $16c$ special positions forming an infinite network of corner-sharing MF_6 and $M'F_6$ octahedra. This structure favors the spin glass behavior because the two types of magnetic ions M^{2+} and M'^{3+} are randomly distributed in the same crystallographic site.^{14,15}

Based on the modified pyrochlore crystalline structure and using the method of site group analysis proposed by Rousseau *et al.*,¹³ the distribution of the degrees of freedom in terms of the irreducible representations of the O_h factor group was calculated and shown in Table I. According to the character table of the O_h point group, acoustic and infrared active modes belong to the F_{1u} representation, while A_{1g} , E_g , and F_{2g} irreducible representations are Raman active. The polarizability tensors of the Raman-active modes are as follows:

$$\begin{aligned}
 A_{1g}: & \begin{pmatrix} a & \cdot & \cdot \\ \cdot & a & \cdot \\ \cdot & \cdot & a \end{pmatrix}, \\
 E_g: & \begin{pmatrix} b & \cdot & \cdot \\ \cdot & -b & \cdot \\ \cdot & \cdot & -2b \end{pmatrix}, \begin{pmatrix} -\sqrt{3}b & \cdot & \cdot \\ \cdot & -\sqrt{3}b & \cdot \\ \cdot & \cdot & \cdot \end{pmatrix}, \\
 F_{2g}: & \begin{pmatrix} \cdot & \cdot & \cdot \\ \cdot & \cdot & d \\ \cdot & d & \cdot \end{pmatrix}, \begin{pmatrix} \cdot & \cdot & d \\ \cdot & \cdot & \cdot \\ d & \cdot & \cdot \end{pmatrix}, \begin{pmatrix} \cdot & d & \cdot \\ d & \cdot & \cdot \\ \cdot & \cdot & \cdot \end{pmatrix}.
 \end{aligned} \tag{1}$$

In addition to the crystallographic axes, crystals with faces perpendicular to $[110]$ and $[1\bar{1}0]$ were cut. These directions will henceforth be denoted x' and y' , respectively. The relative intensity of the modes, summarized in Table II, can be calculated from the Raman polarizability tensors by using the following relation:

$$I \propto |\mathbf{e}_o^\dagger \cdot \alpha \cdot \mathbf{e}_i|^2, \tag{2}$$

where α are the polarizability tensors given in (1) and, \mathbf{e}_i and \mathbf{e}_o are the incoming and outgoing light polarization directions, respectively. Notice that when the incident and outgoing beams are both polarized parallel to the same crystallographic axis a mixture of phonons belonging to A_{1g} and E_g irreducible representations is observed, while if they are polarized parallel to different crystallographic axes the F_{2g} modes are detected. In order to discriminate between A_{1g} and E_g modes, light polarized along to x' and y' can be used. In fact, the crossed polarization geometry $z(x'y')\bar{z}$ allows the observation of E_g modes only, while in the $z(x'x')\bar{z}$ geometry all Raman-active modes would be detected. In this way, polarized Raman measurements in the first three scattering geometries of Table II suffice to distinguish between the three allowed symmetries of Raman-active modes.

IV. RESULTS

A. Raman scattering

Raman spectra were recorded in three backscattering polarization geometries $z(xx)\bar{z}$, $z(x'y')\bar{z}$, and $z(xy)\bar{z}$. These spectra are shown in Fig. 1. According to Sec. III, in the $z(xx)\bar{z}$ configuration [Fig. 1(a)], only two vibrational modes are predicted: $A_{1g} \oplus E_g$. Nevertheless, thirteen bands were

TABLE II. Intensity of the Raman active modes in different backscattering configurations for cubic structures.

Configuration	A_{1g}	E_g	F_{2g}
$z(xx)\bar{z}$	a^2	$4b^2$	0
$z(xy)\bar{z}$	0	0	d^2
$z(x'y')\bar{z}$	0	b^2	0
$z(x'x')\bar{z}$	a^2	$3b^2$	d^2

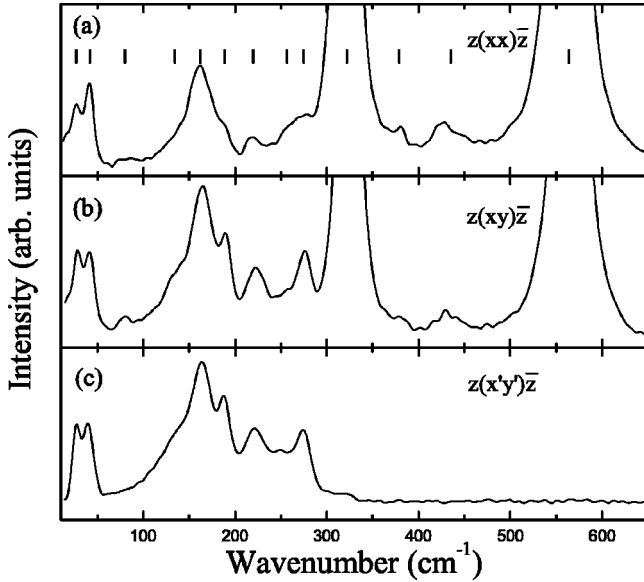


FIG. 1. Raman spectra of CsInMgF₆ in (a) $z(xx)\bar{z}$, (b) $z(xy)\bar{z}$, and (c) $z(x'y')\bar{z}$ scattering geometries.

observed in this configuration. The same peculiar behavior is observed in the $z(xy)\bar{z}$ configuration, given in Fig. 1(b), where the same thirteen modes can be identified, when only four modes belonging to the F_{2g} representation were expected. In the $z(x'y')\bar{z}$ crossed polarization [Fig. 1(c)], where just one E_g mode should be present, we can see clearly the presence of nine modes in the spectrum. Table III lists the observed bands for the three above scattering configurations. The random distribution of Mg²⁺ and In³⁺ ions in the octahedral sites would be responsible for the difference between the observed and predicted numbers of vibrational modes. The effect of the occupational disorder of the octahedral sites in the vibrational spectra will be discussed in detail in Sec. V.

TABLE III. Wave numbers of the Raman bands observed in CsInMgF₆ single crystals, at room temperature in different scattering geometries.

Wave number (cm ⁻¹)		
$z(xx)\bar{z}$	$z(xy)\bar{z}$	$z(x'y')\bar{z}$
27	27	27
42	43	40
80	80	
134	135	136
162	165	165
189	190	189
220	223	221
257	253	253
275	273	275
322	323	320
379	382	
435	432	
564	565	

TABLE IV. Dispersion parameters for the best fit to the reflectivity data of CsInMgF₆ crystals at 300 K.

ω_{TO} (cm ⁻¹)	γ_{TO} (cm ⁻¹)	ω_{LO} (cm ⁻¹)	γ_{LO} (cm ⁻¹)	$\Delta\epsilon_{TO}$
34	9	41	3	13.643
42	3	58	6	0.421
119	31	120	40	0.000
147	65	179	29	2.894
196	16	201	16	0.162
239	33	250	35	0.440
280	68	297	53	0.482
315	46	324	52	0.138
368	37	376	22	0.461
378	23	401	70	0.028
407	31	408	65	0.004
432	46	437	33	0.052
491	18	496	59	0.373
498	32	551	118	0.071
555	68	580	45	0.006
$\epsilon_\infty = 2.168$		$\epsilon_0 = 21.343$		

B. Infrared reflectivity

The infrared dielectric function was determined from the reflectivity spectrum by using the four parameters semi-quantum model.^{17,18} According to this model, the complex dielectric constant is expressed in terms of the infrared-active modes as follows:

$$\epsilon(\omega) = \epsilon_\infty \prod_j \frac{\omega_{jLO}^2 - \omega^2 + i\omega\gamma_{jLO}}{\omega_{jTO}^2 - \omega^2 + i\omega\gamma_{jTO}}, \quad (3)$$

where ω_{jTO} and ω_{jLO} correspond to the resonance frequencies of the j th transversal and longitudinal modes, respectively, and γ_{jTO} and γ_{jLO} are the corresponding damping factors. ϵ_∞ is the dielectric constant due to the electronic polarization. For normal incidence, the infrared reflectivity \mathbf{R} and the dielectric function are related by

$$\mathbf{R} = \left| \frac{\sqrt{\epsilon} - 1}{\sqrt{\epsilon} + 1} \right|^2. \quad (4)$$

Table IV lists the frequencies of LO and TO IR-modes from the best fit of Eq. (3) to the experimental reflectivity curve. The experimental data and adjustment curve are presented in Fig. 2. The oscillator strength $\Delta\epsilon_j$ of the j th transversal mode can be directly deduced from the LO-TO splitting, through the relation

$$\Delta\epsilon_j = \frac{\epsilon_\infty}{\omega_{jTO}^2} \times \frac{\prod_k \omega_{kLO}^2 - \omega_{jTO}^2}{\prod_{k \neq j} \omega_{kTO}^2 - \omega_{jTO}^2}. \quad (5)$$

Furthermore, the static dielectric constant can be obtained by adding up the strength of all oscillators, i.e.,

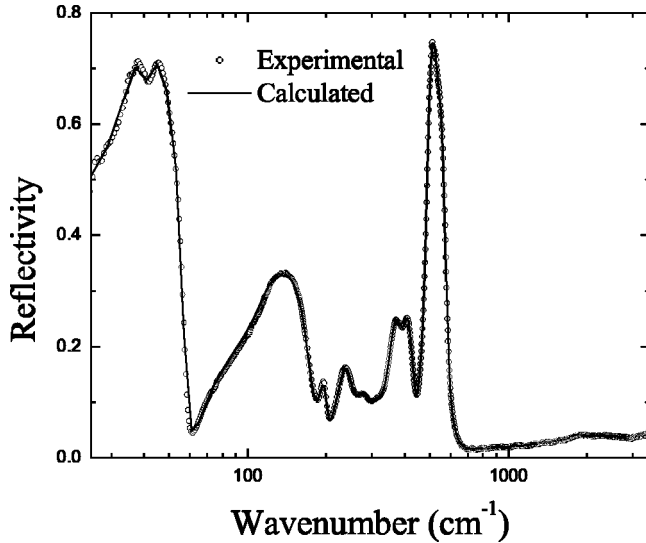


FIG. 2. Infrared reflectivity data of CsInMgF₆ single crystals and the best fit by the four parameters semiquantum model.

$$\varepsilon_0 = \varepsilon_\infty + \sum_j \Delta\varepsilon_j. \quad (6)$$

As can be observed from Table IV, fifteen bands were identified in the reflectivity spectrum. This number is large when compared with the five F_{1u} modes predicted by the group theory analysis. Again, the origin of this behavior should be the disorder of the Mg²⁺ and In³⁺ ions and will be discussed in the following section.

V. DISCUSSIONS

The vibrational spectra obtained previously will be discussed in the framework of the random distribution of Mg²⁺ and In³⁺ ions in the octahedral sites of the CsInMgF₆ pyrochlore. Differently from x-ray diffraction, where disorder is observed through the average of the scattering factors, the vibrational spectra are affected not only by the atomic species distribution but also by the different interatomic interactions. Due to this fact, the interpretation of the vibrational spectra of disordered crystals is always arduous. In some solid solutions it is possible to observe a shift of the bands proportional to the concentration of the dopant (*one mode behavior*),^{19,20} mainly due to the variation of the effective mass. This is not the case here because, in this model, the number of vibrational modes should be preserved, in contrast to our observations. On the other hand, in compounds where two atomic species can occupy the same crystallographic lattice site there could be a doubling of the bands originated in the vibrational modes involving these atoms (two mode behavior).^{21,22} This hypothesis is ruled out here because disordered cations do not contribute to the irreducible representation with any Raman-active representation (see Table I). Thus, disorder-induced band splitting could be expected only in the infrared spectra with addition of, at most, two modes, which does not explain the larger number of infrared bands observed. Notice that the disordered ions, Mg²⁺ and In³⁺ in our case, differ not only in their atomic mass, but

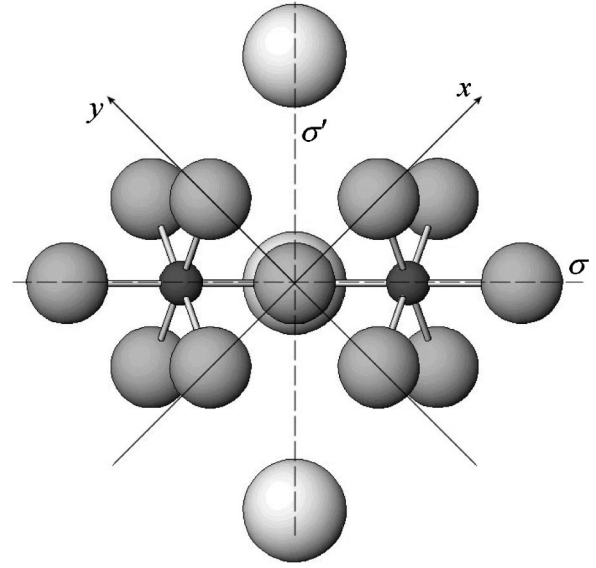


FIG. 3. Fluorine first neighbors coordination. Large, medium, and small spheres represent cesium, fluorine and indium or magnesium atoms, respectively. Dashed lines represent mirror planes (σ and σ').

also in their valences. This situation produces a much more complex behavior, since, using the simple harmonic oscillator model, both the mass and coupling constant change simultaneously. This effect is enhanced due to the fact that the MF₆ octahedra are not isolated, but linked by fluorine ions, producing the coupling of the vibrational modes of the octahedral groups.

In order to explain the enlarged number of vibrational modes observed, we propose a model which considers a symmetry breakdown due to the cation disorder. First, we will consider the first-neighbor coordination polyhedrum of the atomic species, in order to identify the effect of the disorder on these polyhedra. In this way, while cesium cations are located at the center of regular octahedra, disordered M²⁺ and M'³⁺ ions also occupy the center of fluorine octahedra, but they have a trigonal distortion and the M-F distance is approximately half that the Cs-F distance. In addition, fluorine ions are shared by two MF₆ octahedra. Indeed, in a first neighbor analysis, cesium, M and M' ions are always surrounded by six fluorine anions and their coordination polyhedra are not affected by the occupational disorder. Differently, fluorine anions first neighbors are always the disordered M and M' ions. As a consequence, disorder-induced symmetry breakdown only result from these sites.

According to the modified pyrochlore structure, fluorine anions are located at sites with C_{2v} symmetry. Figure 3 shows the first neighbors coordination of the fluorine ions, where the mirror planes of the C_{2v} point group are indicated by dashed lines and the C₂ axis is perpendicular to the plane of the figure. Notice that if the centers of the two octahedra are occupied by the same ion (M or M'), these sites are related by the σ' mirror and the C₂ axis, while the σ mirror transforms each M site into itself. As a consequence, if the central ions are different, both the σ' mirror and C₂ axis disappear, while the σ mirror is retained. Thus, the site sym-

TABLE V. Irreducible representations of the $R\bar{3}m$ (D_{3d}^5) subgroup of the CsInMgF₆ structure.

Ion	Wyckoff site	Symmetry	Irreducible representations
Cs	2c	C_{3v}	$A_{1g} \oplus A_{2u} \oplus E_g \oplus E_u$
(Mg/In) ₁	1a	D_{3d}	$A_{2u} \oplus E_u$
(Mg/In) ₂	3d	C_{2h}	$A_{1u} \oplus 2A_{2u} \oplus 3E_u$
F ₁	6h	C_s	$2A_{1g} \oplus A_{1u} \oplus A_{2g} \oplus 2A_{2u} \oplus 3E_g \oplus 3E_u$
F ₂	6h	C_s	$2A_{1g} \oplus A_{1u} \oplus A_{2g} \oplus 2A_{2u} \oplus 3E_g \oplus 3E_u$
	Total		$\Gamma = 5A_{1g} \oplus 3A_{1u} \oplus 2A_{2g} \oplus 8A_{2u} \oplus 7E_g \oplus 11E_u$
	Acoustic		$\Gamma_{ac} = A_{2u} \oplus E_u$
	Raman		$\Gamma_R = 5A_{1g} \oplus 7E_g$
	Infrared		$\Gamma_{IR} = 7A_{2u} \oplus 10E_u$

metry of the fluorine anion is reduced to C_s . Since the symmetry reduction is accomplished by the loss of the same symmetry operations of the space group, the new crystal symmetry must be a $Fd\bar{3}m$ subgroup. In particular, the loss of the C_2 axis corresponds to the loss of the C_4 axis of the O_h point group; consequently C_4 axes are also lost. The remaining symmetry operation determines the trigonal $R\bar{3}m$ (D_{3d}^5) space group, which is subgroup of the $Fd\bar{3}m$ space group. There are four equivalent subgroups, whose principal axes are oriented along the major cube diagonals. Since, the atoms in all subgroups have the same site symmetries, the irreducible representations of each subgroup are equals. Thus, Table V shows the factor group analysis for the $R\bar{3}m$ structure, and lists the activity of the modes in Raman scattering (Γ_R) and infrared reflectivity (Γ_{IR}).

Notice that in the D_{3d} point group, A_{2u} and E_u irreducible representations are infrared active. Thus, seventeen bands are predicted in the reflectivity spectra. This number agrees very well with the fifteen bands observed experimentally, suggesting that the proposed method seems to be adequate to explain the anomalous CsInMgF₆ vibrational spectra.

Let us extend this analysis to the Raman spectra in order to explain the larger number of observed bands as compared to the factor group of the O_h point group and their dependence with the scattering geometry. First, keep in mind that there are four equivalent trigonal subgroups, whose principal axes are oriented along the $[111]$, $[1\bar{1}1]$, $[\bar{1}\bar{1}1]$, and $[\bar{1}11]$ directions. Although the occupational disorder should reduce the site symmetries, the crystal still belongs to a cubic system. Hence, no trigonal subgroups should be privileged and the complete crystal should be imagined as a set of trigonal cells randomly oriented along the cube diagonals.

In order to analyze the Raman spectra in the trigonal base, we must transform the polarization directions to this new base. Henceforth, we will use the subscripts c and t to indicate cubic and trigonal bases, respectively. Let us do this for the subgroup oriented along the $[111]$ cube diagonal (symbolized as d), whose lattice parameters are

$$\mathbf{a}_t = -\frac{1}{2} \mathbf{a}_c + \frac{1}{2} \mathbf{c}_c, \quad (7)$$

$$\mathbf{b}_t = -\frac{1}{2} \mathbf{a}_c - \frac{1}{2} \mathbf{b}_c, \quad (8)$$

$$\mathbf{c}_t = \mathbf{a}_c + \mathbf{b}_c + \mathbf{c}_c. \quad (9)$$

Fixing the last two vectors and replacing \mathbf{a}_t by the cross product of (\mathbf{b}_t and \mathbf{c}_t), we choose a set of principal axes as defined by Nye.²⁴ The unitary matrix that rotate cubic to trigonal axes is given by

$$\mathbf{R} = \begin{pmatrix} \frac{1}{\sqrt{6}} & \frac{1}{\sqrt{6}} & -\sqrt{\frac{2}{3}} \\ -\frac{1}{\sqrt{2}} & \frac{1}{\sqrt{2}} & 0 \\ \frac{1}{\sqrt{3}} & \frac{1}{\sqrt{3}} & \frac{1}{\sqrt{3}} \end{pmatrix}. \quad (10)$$

Even though the trigonal subgroups are randomly oriented along the cube diagonals, the light polarizations used experimentally are at well defined angles related to the different trigonal bases. In consequence, the Raman intensities in the different scattering geometries can be calculated by rotating the corresponding polarizability tensors. In terms of the principal axes of the trigonal structure, the polarizability tensors of the irreducible representations of the D_{3d} point group are given by²³

$$A_{1g}: \begin{pmatrix} a & \cdot & \cdot \\ \cdot & a & \cdot \\ \cdot & \cdot & b \end{pmatrix},$$

$$E_g: \begin{pmatrix} c & \cdot & \cdot \\ \cdot & -c & d \\ \cdot & d & \cdot \end{pmatrix}, \begin{pmatrix} \cdot & -c & -d \\ -c & \cdot & \cdot \\ -d & \cdot & \cdot \end{pmatrix}. \quad (11)$$

Now, the intensity of the Raman bands in the different scattering geometries can be calculated according to Eq. (2), using the rotation matrix (10):

$$I \propto |\mathbf{e}_0^\dagger \cdot \mathbf{R}^\dagger \cdot \alpha_t \cdot \mathbf{R} \cdot \mathbf{e}_i|^2. \quad (12)$$

TABLE VI. Raman intensities calculated for each polarizability tensor of the D_{3d} point group in chosen scattering geometries. The Calculations were carried out for the trigonal subgroup whose principal axis is oriented along the [111] direction.

	A_{1g}	$E_g^{(1)}$	$E_g^{(2)}$
xx	$\frac{(2a+b)^2}{9}$	$\frac{(c+\sqrt{6}d)^2}{9}$	$\frac{(\sqrt{3}c-\sqrt{2}d)^2}{9}$
xy	$\frac{(a-b)^2}{9}$	$\frac{4c^2}{9}$	$\frac{2d^2}{9}$
$x'x'$	$\frac{4(a+2b)^2}{9}$	$\frac{4c^2}{9}$	$\frac{32d^2}{9}$
$x'y'$	0	$\frac{8d^2}{3}$	$\frac{4c^2}{3}$
$x'z$	$4b^2$	0	$2d^2$
dd	$9b^2$	0	0

Thus, in our example, the intensity of the bands belonging to the trigonal A_{1g} representation in the $z(xx)\bar{z}$ and $z(x'y')\bar{z}$ scattering geometries are

$$I_{xx} \propto (100) \cdot \mathbf{R}^\dagger \cdot \begin{pmatrix} a & \cdot & \cdot \\ \cdot & a & \cdot \\ \cdot & \cdot & b \end{pmatrix} \cdot \mathbf{R} \cdot \begin{pmatrix} 1 \\ 0 \\ 0 \end{pmatrix} = \frac{1}{9} (2a+b)^2, \quad (13)$$

$$I_{x'y'} \propto (110) \cdot \mathbf{R}^\dagger \cdot \begin{pmatrix} a & \cdot & \cdot \\ \cdot & a & \cdot \\ \cdot & \cdot & b \end{pmatrix} \cdot \mathbf{R} \cdot \begin{pmatrix} 1 \\ \bar{1} \\ 0 \end{pmatrix} = 0. \quad (14)$$

Table VI lists the Raman intensities calculated by using Eq. (12) in several scattering geometries. As usual, null intensities of these table could help us to identify the phonons belonging to the different irreducible representations. Thus, A_{1g} and E_g phonons should be observed separately using the dd and $x'y'$ scattering configurations, respectively. This analysis was accomplished by the trigonal subgroup whose principal axis is oriented along the [111] direction but, as it was pointed out, there are four equivalent trigonal subgroups. As a consequence, no trigonal subgroup is privileged and the Raman intensity must be the average of all possible orientations, that is

$$\bar{I} \propto \frac{1}{4} \sum_{i=1}^4 |\mathbf{e}_o^\dagger \cdot \mathbf{R}_i^\dagger \cdot \alpha_i \cdot \mathbf{R}_i \cdot \mathbf{e}_i|^2. \quad (16)$$

The averaged Raman intensities calculated using Eq. (16) are given in Table VII for the scattering geometries listed in Table VI. Based on these results we are now able to analyze the Raman spectra obtained experimentally. According to Table VII, in the $z(xx)\bar{z}$ configuration both Raman-active irreducible representations have nonzero intensities and twelve bands are expected. An equivalent situation is predicted for the $z(xy)\bar{z}$ spectrum, where the number of bands

TABLE VII. Averaged Raman intensities calculated in several scattering geometries.

	A_{1g}	$E_g^{(1)}$	$E_g^{(2)}$
xx	$\frac{4(2a+b)^2}{9}$	$\frac{4(c^2+6d^2)}{9}$	$\frac{4(3c^2+2d^2)}{9}$
xy	$\frac{4(a-b)^2}{9}$	$\frac{16c^2}{9}$	$\frac{8d^2}{9}$
$x'x'$	$8a^2 + \frac{8(a+2b)^2}{9}$	$\frac{80c^2}{9}$	$\frac{64d^2}{9}$
$x'y'$	0	$\frac{32d^2}{3}$	$\frac{16c^2}{3}$
$x'z$	$\frac{8(11a^2+2ab+5b^2)}{9}$	$\frac{4(22c^2+3d^2)}{9}$	$\frac{4(6c^2+17d^2)}{9}$
dd	$9b^2 + \frac{(8a+b)^2}{3}$	$\frac{16(2c^2+d^2)}{3}$	$\frac{16(2c^2+d^2)}{3}$

must be the same as before but differences in the relative intensities should be observed. In $z(x'x')\bar{z}$ and $z(x'z)\bar{z}$ scattering geometries, some subgroup orientations present null intensity in one of the components of the doubly degenerate E_g representations (see Table VI). However, when we average all possible orientations, as shown in Table VII, both A_{1g} and E_g representations should be observed in the spectra. According to Table VI, in the dd configuration, it seems to be possible to separate the A_{1g} bands, but when the intensity of E_g modes is averaged using equation 16, E_g modes become active in this scattering geometry. For that reason, crystals cut with faces containing the [111] direction do not provide any additional information. The most interesting configuration is the $z(x'y')\bar{z}$, since for all orientation of the trigonal subgroups, the intensity of the A_{1g} bands are zero and, thus, the averaged intensity is also null. Based on this, in the $z(x'y')\bar{z}$ spectrum, only the seven E_g bands should be present.

By comparing our experimental results with the new predictions we observe a remarkable agreement. In the $z(xx)\bar{z}$ and $z(xy)\bar{z}$ spectra thirteen bands were observed, while twelve bands are predicted by our model. Furthermore, these spectra are very similar, in good agreement with our predictions of Table VII. Notice that, in the $z(x'y')\bar{z}$ spectrum we have eight bands, after discarding the band at 322 cm^{-1} which is a leak of the intense band observed in the $z(xx)\bar{z}$ spectra at the same wave number. The band located at 136 cm^{-1} was introduced in order to improve the fit, but it is unusually wide and should be considered as an asymmetric contribution to the band that peaks at 165 cm^{-1} . Actually, at approximately this wave number, the vibrational modes associated to the (M, M') -F bonds are expected, which should produce a *two modes*-like behavior enlarging the band. Based on this consideration, bands located above 300 cm^{-1} , observed only in Figs. 1(a) and 1(b), can be associated to A_{1g} phonons. The remaining A_{1g} band is located at 80 cm^{-1} and corresponds to the translation of the cesium cation as it was predicted by Table V. On the other hand, the bands observed

TABLE VIII. Classification of the observed Raman bands in CsInMgF₆ according to the irreducible representations of the D_{3d} point group.

Wave number (cm ⁻¹)	
A_{1g}	E_g
80	27
322	40
379	136
435	165
564	189
	221
	253
	275

in the $z(x'y')\bar{z}$ spectrum correspond to E_g phonons and are at the same wave number than those of the $z(xx)\bar{z}$ and $z(xy)\bar{z}$ spectra, in complete agreement with our model. Even though Table VII predicts the same number of bands in the $z(xx)\bar{z}$ and $z(xy)\bar{z}$ spectra, the relative intensities of A_{1g} and E_g bands in these spectra should be different, since each component of the E_g modes does not contribute equally to the main intensity. This result is confirmed by comparing the low wavenumber region of Figs. 1(a) and 1(b), which is mostly associated to E_g phonons. Notice that, in Table VII, the intensities of the components of the E_g phonons in $z(xy)\bar{z}$ and $z(x'y')\bar{z}$ are related by a multiplication factor. Thus, relative intensities of E_g bands need to be similar in both spectra, as it can be observed in Fig. 1(c). Finally, Table VIII presents the proposed classification of the observed Raman modes in the irreducible representations of the trigonal D_{3d} group.

On the basis of the above model, the intensities of the infrared bands can be calculated, since they are proportional to the projection of the polar vector \mathbf{P} on the polarization direction

$$I_{\text{IR}} \propto |\mathbf{P} \cdot \mathbf{R} \cdot \mathbf{e}_i|^2. \quad (17)$$

Once in the D_{3d} point group the A_{2u} phonons are polarized along the z_t direction and the doubly degenerated E_u in the $x_t y_t$ plane (forming an angle θ with the x_t axis), the polar vectors can be represented by

$$A_{2u}: (0, 0, p_z), \quad (18)$$

$$E_u: (p_{xy} \cos \theta, p_{xy} \sin \theta, 0). \quad (19)$$

After averaging over all orientations of the trigonal subgroups, the calculated infrared intensities are presented in Table IX. Notice that, the relative intensities of the infrared bands in the x and x' polarizations are completely equivalent and no dependence would be expected from polarized measurements. On the other hand, by choosing one of the cube diagonal, we have a slightly different situation, where all infrared bands are allowed but the A_{2u} and E_u relative intensities differs from the first two configurations. However, this

TABLE IX. Averaged infrared intensities calculated in different directions of the light polarization.

\bar{x}	$\frac{4}{3} \{ [1 - \frac{1}{2} \cos(2\theta)] p_{xy}^2 + p_z^2 \}$
\bar{x}'	$\frac{8}{3} \{ [1 - \frac{1}{2} \cos(2\theta)] p_{xy}^2 + p_z^2 \}$
\bar{d}	$4(p_{xy}^2 + p_z^2)$

difference is not sufficient to allow for the distinction between A_{2u} (p_z) and E_u (p_x, p_y) modes, since the sum of the $\Delta \varepsilon_j$ strength should give nearly the same ($\varepsilon_o - \varepsilon_\infty$) value, irrespective of the particular direction.

Based on our model, we were able to explain the anomalous behavior of the vibrational spectrum of the CsInMgF₆ pyrochlore. The increase in the number of Raman and infrared active modes due the symmetry reduction can be understood by considering the correlation between the irreducible representations of the O_h and its D_{3d} subgroup. Due to this correlation, all triply degenerated representations of the O_h point group break into one unidimensional and one bidimensional representation. In the case of Raman-active phonons, in addition to the splitting of the F_{2g} representations, the bidimensional component of the F_{1g} representation, which is silent, transforms into a Raman active representation. On the other hand, the infrared spectra receive additional contributions from the silent A_{2u} , E_u , and F_{2u} irreducible representations. In this way, we can conclude that the large number of vibrational bands is due to the breaking of the degeneration of tridimensional representations and the activation of the silent representations of the O_h point group, due to the disorder-induced symmetry lowering.

Let us discuss briefly the consequences of the symmetry lowering on the magnetic properties of modified pyrochlores. As it was pointed out, the high geometrical frustration observed in this kind of materials is originated from the lack of a spin configuration that satisfies all six antiferromagnetic interactions in a single tetrahedron. However, experimental^{25,26} and theoretical^{11,27,28} results showed at least one magnetic ordered structure in modified pyrochlore crystals. This structure lies in the ($[hh0]_c, [00l]_c$) plane and is related to an ordered phase where consecutive tetrahedra are in phase. By considering the symmetry lowering proposed in this work, it should be noticed that the plane of the magnetic structure transforms into the ($[h00]_t, [00l]_t$) in the trigonal subgroup. From a structural point of view, in the pyrochlore structure all magnetic ion lie in sites with symmetry D_{3d} with their principal axis along the $\langle 111 \rangle_c$ -type directions. However, the symmetry lowering reduces the symmetry of same magnetic sites to C_{2h} , whose principal axes are perpendicular to the $\langle 111 \rangle_c$ -type directions. Thus, the magnetic structure can be decomposed into a component parallel to the principal axis of the D_{3d} sites and a component lying on the plane determined by the principal axes of the C_{2h} sites. Furthermore, it was noticed that the magnetic cross section of the ($[hh0]_c, [00l]_c$) plane is similar to that of the two-dimensional *kagomé* lattice.^{29,30} This result should be better understood observing that the plane determined by the principal axes of the C_{2h} sites is exactly a two-dimensional *kagomé* lattice.

VI. CONCLUSIONS

Polarized Raman scattering and infrared reflectivity measurements allowed us to determine the vibrational spectra of the modified pyrochlore CsInMgF_6 . A large number of vibrational bands was observed, which can not be explained on the basis of the factor group analysis of the O_h point group. By considering the occupational disorder of Mg^{2+} and In^{3+} metallic ions, a symmetry lowering effect was proposed which reduces the O_h point group to the D_{3d} one. Furthermore, by using the symmetry properties of the Raman polarizability tensors, the atypical band distribution and symmetries were successfully explained. Despite the apparent

correlation between the anomalous vibrational spectra and the magnetic behavior of highly frustrated modified pyrochlore antiferromagnets, this is a complex problem and detailed calculations must be done in order to determine the real consequences of the symmetry lowering on the general properties of this system. Work in this direction is in progress.

ACKNOWLEDGMENTS

This work was partially supported by the Brazilian government agencies CNPq, FAPEMIG, and FUNCAP.

-
- ¹A.P. Ramirez, *Annu. Rev. Mater. Sci.* **24**, 453 (1994).
²P. Schiffer and A.P. Ramirez, *Comments Condens. Matter Phys.* **18**, 21 (1996).
³M.J. Harris and M.P. Zinkin, *Mod. Phys. Lett. B* **10**, 417 (1996).
⁴R. Moessner and J.T. Chalker, *Phys. Rev. B* **58**, 12 049 (1998).
⁵N.N. Greenwood, A.T. Howe, and F. Menil, *J. Chem. Soc. A* **13**, 2218 (1971).
⁶A. Tressaud, R. dePape, and J. Portier, *C. R. Acad. Sci.* **40**, 1 (1981).
⁷G. Ferey, M. Leblanc, and R. de Pape, *J. Solid State Chem.* **40**, 1 (1981).
⁸M.A. Subramanian, W.J. Marshall, and R.L. Harlow, *Mater. Res. Bull.* **31**, 585 (1996).
⁹J. Villain, *Z. Phys. B: Condens. Matter* **33**, 31 (1979).
¹⁰T. Zeiske, M.J. Harris, and M.P. Zinkin, *Physica B* **234**, 766 (1997).
¹¹M.P. Zinkin, M.J. Harris, and T. Zeiske, *Phys. Rev. B* **56**, 11 786 (1997).
¹²S.P.S. Porto and J.F. Scott, *Phys. Rev. B* **157**, 716 (1967).
¹³D.L. Rousseau, R.P. Bauman, and S.P.S. Porto, *J. Raman Spectrosc.* **10**, 253 (1981).
¹⁴W. Kurts, R. Geller, H. Dachs, and P. Covert, *Solid State Commun.* **18**, 1479 (1976).
¹⁵F. Varret and G. Courbion, *Rev. Phys. Appl.* **15**, 1149 (1980).
¹⁶R. Hoopé and R. Jesse, *Z. Anorg. Allg. Chem.* **402**, 29 (1973).
¹⁷F. Gervais and P. Echegut, in *Incommensurate phases in dielectrics*, edited by R. Blinc and A. P. Levanyuk (North Holland, Amsterdam, 1986), p. 337.
¹⁸D. D. Meneses, desouza@cncrs-orleans.fr, IRFit2.0 adjustment program, Orleans University, Orleans, France, 1999.
¹⁹P. Daniel, J. Toulouse, and M. Rousseau, *Eur. Phys. J.: Appl. Phys.* **5**, 33 (1999).
²⁰S.G. Yu, K.W. Kim, L. Bergman, M. Dutta, M.A. Stroschio, and J.M. Zavada, *Phys. Rev. B* **58**, 15 283 (1998).
²¹R. Mouras, M.D. Fontana, P. Bourson, and A.V. Postnikov, *J. Phys.: Condens. Matter* **12**, 5053 (2000).
²²R.L. Moreira, F.M. Matinaga, and A. Dias, *Appl. Phys. Lett.* **78**, 428 (2001).
²³W. Hayes and R. Loudon, *Scattering of Light by Crystals* (Wiley-Interscience, New York, 1978).
²⁴J. F. Nye, *Physical Properties of Crystal: Their Representation by Tensor and Matrices* (Clarendon Press, Oxford, 1957).
²⁵M.J. Harris, M.P. Zinkin, Z. Tun, B.M. Wanklyn, and I.P. Swainson, *Phys. Rev. Lett.* **73**, 189 (1994).
²⁶M.J. Harris, S.T. Bramwell, D.F. McMorrow, T. Zeiske, and K.W. Godfrey, *Phys. Rev. Lett.* **79**, 2554 (1997).
²⁷B. Canals and C. Lacroix, *Phys. Rev. Lett.* **80**, 2933 (1998).
²⁸B. Canals and C. Lacroix, *Phys. Rev. B* **61**, 1149 (2000).
²⁹P. Lecheminant, B. Bernu, C. Lhuillier, L. Pierre, and P. Sindzingre, *Phys. Rev. B* **56**, 2521 (1997).
³⁰D.A. Garanin and B. Canals, *Phys. Rev. B* **59**, 443 (1999).